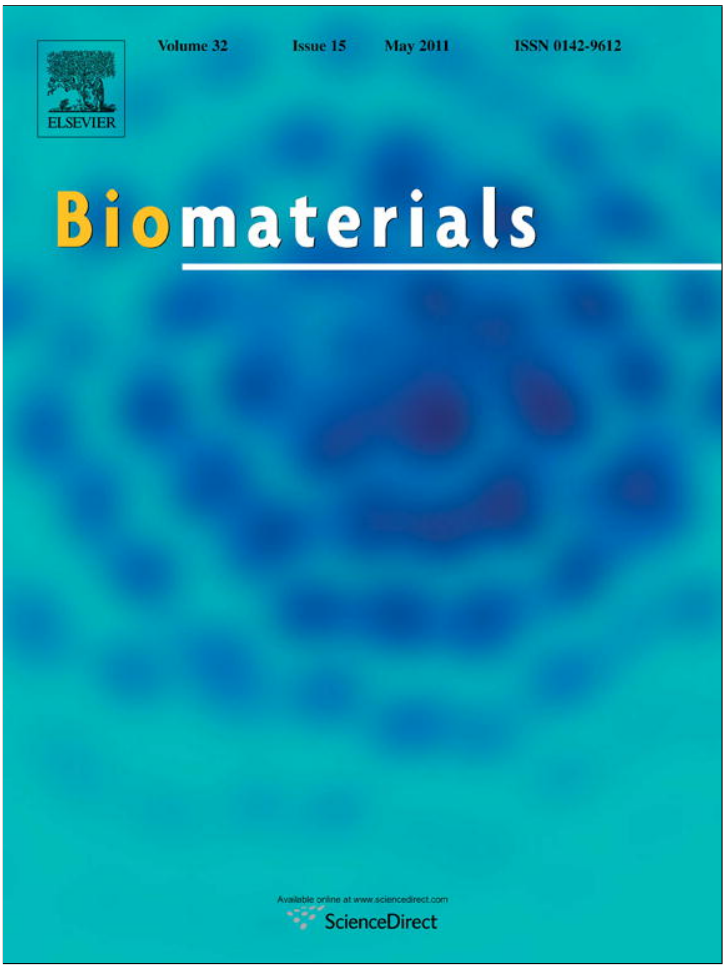

Biomaterials 32 (2011) 3875–3882

Contents lists available at ScienceDirect

Biomaterials

journal homepage: www.elsevier.com/locate/biomaterials

The use of polyethylenimine-grafted graphene nanoribbon for cellular delivery of locked nucleic acid modified molecular beacon for recognition of microRNA

Haifeng Dong [a], Lin Ding [a], Feng Yan [b,*], Hanxu Ji [a], Huangxian Ju [a,*]

[a] Key Laboratory of Analytical Chemistry for Life Science (Ministry of Education of China), Department of Chemistry, Nanjing University, Nanjing 210093, PR China
[b] Jiangsu Institute of Cancer Prevention and Cure, Nanjing 210009, PR China

ARTICLE INFO

Article history:
Received 17 October 2010
Accepted 1 February 2011
Available online 26 February 2011

Keywords:
Graphene nanoribbons
Nonviral gene vector
Locked nucleic acid
MicroRNA
Polyethylenimine
Cell transfection

ABSTRACT

A simple nanocarrier of polyethylenimine-grafted graphene nanoribbon (PEI-g-GNR) was proposed as an effective gene vector. The GNR was formed by longitudinally unzipping multiwalled carbon nanotubes (MWCNTs), and treated with strong acids and sonication to obtain surface carboxylic acid groups for graft of PEI via electrostatic assembly. The PEI-g-GNR appeared to protect locked nucleic acid modified molecular beacon (LNA-m-MB) probes from nuclease digestion or single-strand binding protein interaction, thus could be used as a nanocarrier of the probes for more efficient transfection of cells than PEI or PEI-g-MWCNTs due to the large surface area of the GNR and high charge density of PEI. The cytotoxicity and apoptosis induced by the PEI-g-GNR were negligible under optimal transfection conditions. Combining with the remarkable affinity and specificity of LNA to microRNA (miRNA), a delivery system by the LNA-m-MB/PEI-g-GNR was proposed for effectively transferring LNA-m-MB into the cells to recognize the target miRNA. Using HeLa cells as model, a method for detection of miRNA in single cell was developed. These results suggested that PEI-g-GNR would be a promising nonviral vector for in situ detection of gene in cytoplasm and gene therapy in clinical application.

1. Introduction

In recent years, much effort has been made in developing nonviral gene vector systems such as liposomes [1], cationic polymers [2], dendrimers [3], polypeptide [4] and nanomaterials [5,6] for gene therapy. These systems possess promising potentials for large-scale production and better biocompatibility in comparison with the viral carriers. Moreover, new agents including functionalized carbon nanotubes and gold nanoparticles are being continuously and actively explored for more efficiently delivering various molecular cargos into living cells [7–10]. Recently, graphene nanoribbon (GNR), the nanometer-sized elongated strip of single-layer graphene with straight edges [11], has emerged with extensive experimental and theoretical study [12,13], however, few attention has focused on its application in life science. This work studied its potential as a nanocarrier of nonviral gene vector system by its functionalization with polyethylenimine (PEI), a highly cationic-charge density polymer at physiological pH, for loading of nucleic acid probe.

PEI has been recognized as one of the most effective and powerful cationic gene delivery vectors due to its "proton sponge effect" [2,14], which leads to osmotic swelling and burst of the endosmosis to release the loaded nucleic acids to cytoplasm when the amine groups of PEI are protonated [15]. A significant variety of modifications to PEI structure have been exploited in an effort to enhance its transfection efficiency [16,17]. Here locked nucleic acid (LNA), a conformational RNA analog, was used to modify a molecular beacon (MB) for preparation of the nucleic acid probe (LNA-m-MB), which was then loaded on PEI grafted GNR (PEI-g-GNR) via electrostatic assembly for the transfection of cells. The LNA generally contains a furanose ring, which is locked in an RNA-mimicking C3′-endo/N-type conformation [18,19]. The high thermal stability of LNA together with the improved mismatch discrimination has made LNA-modified oligonucleotides a promising candidate for specific recognition and detection of microRNAs (miRNAs) [20–22].

MicroRNAs are small noncoding RNAs (~22 nucleotides in length) within plants, animals and virus genomes [23], which either inhibit translation or lead to transcript degradation of the target or proteolysis of the nascent polypeptide to regulate the expression of the target [24,25]. Therefore, miRNAs play fundamental roles in a wide variety of biological processes including cell differentiation, proliferation, and apoptosis as well as tumorigenesis processes [26–28]. The detection of miRNAs has thus become a rapidly emerging field for further understanding the biochemical function of miRNAs and exploring useful diagnostic and prognostic

* Corresponding authors. Tel./fax: +86 25 83593593.
E-mail addresses: yanfeng2007@sohu.com (F. Yan), hxju@nju.edu.cn (H. Ju).

0142-9612/$ – see front matter © 2011 Elsevier Ltd. All rights reserved.
doi:10.1016/j.biomaterials.2011.02.001

markers of diseases. Recently, some technologies have been developed for the detection of miRNAs [20–22,29–31]. However, the unique characteristics of miRNAs, such as very short length, similar nucleotide sequence and quite low abundance expression levels, make the further improved miRNA profiling techniques become an insistent demand.

The large surface area of the GNR and high charge density of the PEI facilitate the load of LNA on PEI-g-GNR. This work made use of the high "proton sponge effect" of PEI to develop a delivery system for effectively transferring LNA-m-MB into the cells (Fig. 1). The remarkable affinity and specificity of LNA to target miRNAs led to a method for in situ detection of miRNA in single cell.

2. Materials and methods

2.1. Material

MWCNTs (CVD method, purity ≥98%, diameter 20–40 nm, and length 1–2 m) were purchased from Nanoport Co. Ltd. (Shenzhen, China), PEI (25 K) was obtained from Sigma (St. Louis, MO, USA). 3-(4,5-Dimethylthiazol-2-yl)-2,5-diphenyltetrazolium bromide (MTT) and propidium iodide (PI) were from KeyGen Biotech. Co. Ltd. (Nanjing, China), and single-stranded DNA binding protein (SSB) was purchased from Promega (Madison, WI, USA). All solutions were prepared by ultrapure water gained from a millipore water purification system (≥18 MΩ, Milli-Q, Millipore). Phosphate buffered saline (PBS, pH 7.4) containing 136.7 mM NaCl, 2.7 mM KCl, 8.72 mM Na_2HPO_4 and 1.41 mM KH_2PO_4 was sterilized by filtrating with filter unit (Millipore, 0.22-μm pore size). All other reagents were of analytical grade.

The oligonucleotides were purchased from Sangon Biological Engineering Technology & Co. Ltd (Shanghai, China) and purified using high-performance liquid chromatography. Their sequences were:

LNA-m-MB probe for miR-21:

5′FAM-CCTAGCATCaGTcTGaTAaGCtAGCTAGG-DABCYL3′ (lowercase: LNA, uppercase: DNA);

Control MB probe for miR-21:

5′FAM-CCTAGCATCAGTCTGATAAGCTAGCTAGG-DABCYL3′

2.2. Synthesis of GNR

The GNR was synthesized by longitudinal unzipping of MWCNTs according to previous report with some modification [11]. Firstly, MWCNTs (50 mg) were suspended in concentrated H_2SO_4 (50 mL) for a period of 4 h. After adding $KMnO_4$ (250 mg) in this suspension and stirring at room temperature for 1 h, the mixture was heated at 55 °C for 30 min. Continued heating at 65 °C was needed when the reaction was not entirely completed, which was examined by adding 30% H_2O_2 to observe the color change. The temperature was then increased to 70 °C for 5–10 min to stabilize the suspension. Afterwards, the suspension was cooled to room temperature and poured onto 120 mL of ice containing 2 mL of 30% H_2O_2. The obtained mixture was filtrated through a PTFE membrane (0.45 μm pore size), and the solid was stirred in 50 mL of water for 30 min and sonicated for 15 min. Concentrated HCl (20%, 10 mL) was added into the mixture and the mixture was then filtered through a PTFE membrane (0.45-μm pore size). The product was stirred in 50 mL of ethanol for 30 min followed by sonication for 15 min. After addition of ether (100%, 50 mL) into the solution, the mixture was again filtrated through a PTFE membrane (0.45-μm pore size). The obtained product was washed twice with ether (20 mL each time) and dried in vacuo. Transmission electron microscope (TEM, JEM 2100), atomic force microscopy (AFM, Agilent 5500, U.S.A.) and Raman spectra measured with Renishaw-inVia Raman microscope (Renishaw, United Kingdom) were employed to characterize the formation of GNR.

2.3. Preparation and characterization of PEI-g-GNR

The GNR was firstly clipped and functionalized with anionic groups on the surface by combined treatment with 3:1 mixture of concentrated H_2SO_4/HNO_3 acids and sonication for 16 h at 55 °C [32,33]. The resulting acid-treated GNR (1 mg/mL) was mixed with 0.2% PEI aqueous stock solution and sonicated for 1 h. The suspension was then centrifuged at 22,000 g for 6 h to remove large GNR and impurities, and excess PEI was removed through filtration in Millipore Microcon 50,000 molecular weight cut-off spin filter. The obtained PEI-g-GNR solution was stored at a concentration of 4 mg/mL.

Fourier transform infrared (FT-IR) spectra recorded on Nicolet 400 Fourier transform infrared spectrometer (Madison, WI) and electrochemical impedance spectra (EIS) obtained with a PGSTAT30/FRA2 system (Autolab, The Netherlands) were used to assess the properties of the PEI-g-GNR. EIS were measured in 0.1 M KCl solution containing 5 mM $K_3[Fe(CN)_6]/K_4[Fe(CN)_6]$ in the frequency range of 10^{-2}–10^5 Hz with an amplitude of the applied sine wave potential of 5 mV.

2.4. Protective properties of PEI-g-GNR

6 μL of the obtained PEI-g-GNR (4 mg/mL) was mixed with 0.5 μL of LNA-m-MB probe (100 μM) and sonicated for 15 min to prepare LNA-m-MB/PEI-g-GNR conjugates, then the conjugates were treated with DNase I (1 unit) for 30 min, and the fluorescence spectrum was recorded on RF-5301 PC (SHIMDZU). As comparison, the LNA-m-MB probe and control MB probe were treated with DNase I with the same procedure. The interactions of the different probes and SSB protein were investigated by adding 5 equiv. SSB in control MB probe, LNA-m-MB probe and the LNA-m-MB/PEI-g-GNR conjugate solutions for 30 min to observe the fluorescence changes.

2.5. Cell culture

HeLa cells line was kindly provided by the Jiangsu Institute of Cancer Prevention and Cure, Nanjing, China. HeLa cells were cultivated in Dulbecco's modified Eagle's medium (DMEM, GIBCO) supplemented with 10% fetal calf serum, penicillin (100 μg/mL) and streptomycin (100 μg/mL) at 37 °C in a humidified 5% CO_2-containing atmosphere. Cell number was obtained using a Petroff–Hausser cell counter (USA).

2.6. Cytotoxicity assay

After HeLa cells ($\sim 1.0 \times 10^4$) were cultivated in 100 μL media each well of a 96-well plate for 12 h, the media were discarded. Either fresh medium alone or medium containing PEI-g-GNR, PEI-g-MWCNTs, or PEI (24 mg/L) was added to each well of

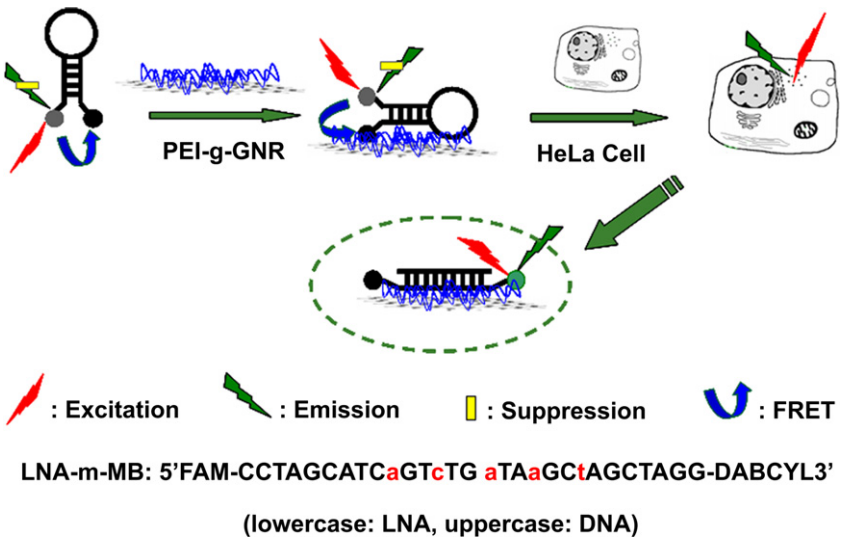

Fig. 1. Transfection of LNA-m-MB probes into HeLa cells via PEI-g-GNR as nanocarrier for detection of target miRNA.

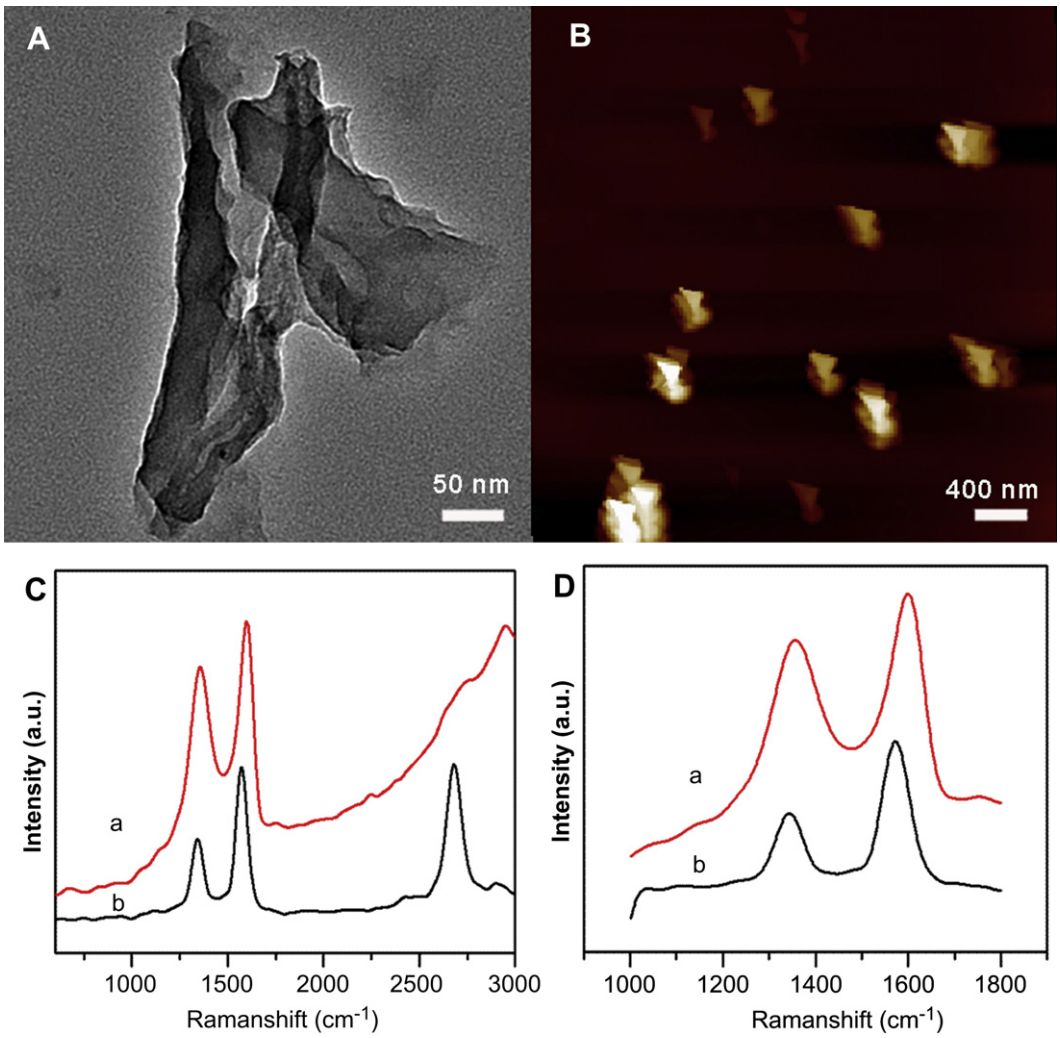

Fig. 2. (A) TEM image, (B) AFM image and (C) Raman spectra of as-prepared GNR, and (D) expanded region of D and G bands from panel (C).

the 96-well plate to cultivate for another 3 h. MTT (20 μL, 5 mg/mL) was then added to each well. After incubation for 4 h, the medium was removed and sodium dodecyl sulfate (150 μL, 0.52 M) was added to each well to solubilize the formazan dye and vortexed. After 15 min, the absorbance of the PEI-g-GNR, PEI-g-MWCNTs and PEI-treated wells and the control wells that were not treated was measured using Hitachi/Roche System Cobas 6000 (Tokyo, Japan) at 490 nm, respectively. The relative cell viability (%) was calculated by $(A_{test}/A_{control}) \times 100$.

2.7. *In vitro transfection*

HeLa cells were seeded on glass cover slides, which were put in DMEM containing ~5×10^4 cells per well in cell culture plates for 12 h, respectively. The media were then discarded, and fresh media (l mL) containing PEI-g-GNR, PEI-g-MWCNTs, and PEI (24 mg/L) were added and incubated for 3 h, respectively. Finally, the cover slides were taken out from the wells, rinsed thoroughly with sterile PBS, and fixed

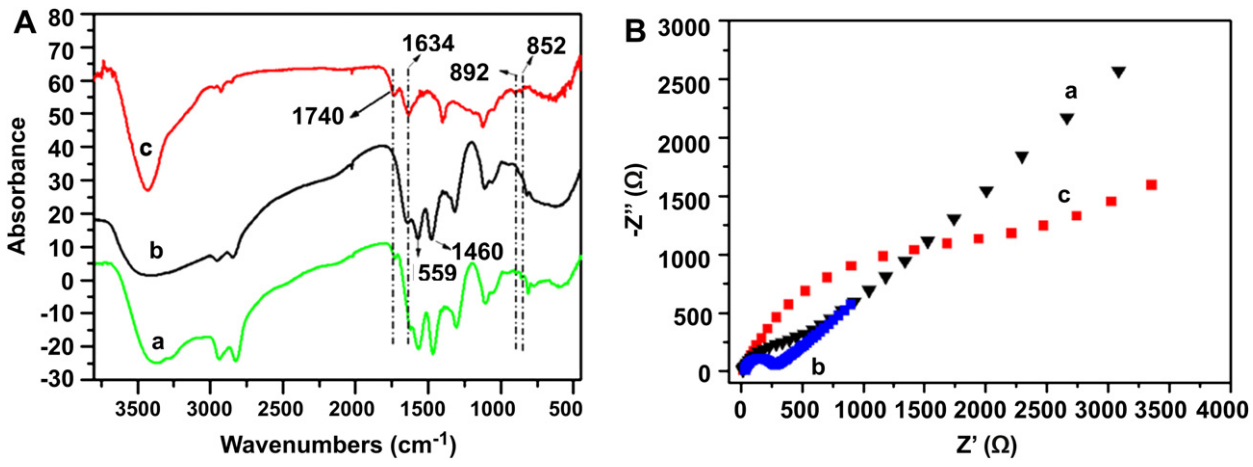

Fig. 3. (A) FT-IR spectra of (a) PEI-g-GNR, (b) PEI and (c) GNR, and (B) EIS of (a) bare, (b) PEI-g-GNR and (c) GNR modified GCEs in 0.1 M KCl containing 5 mM $K_3[Fe(CN)_6]/K_4[Fe(CN)_6]$.

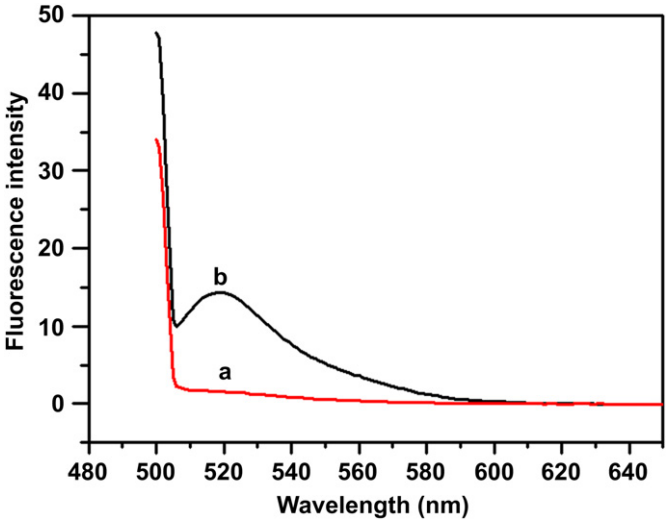

Fig. 4. Emission fluorescence spectra of LNA-m-MB/PEI-g-GNR in (a) absence and (b) presence of 4-fold excess of target cDNA.

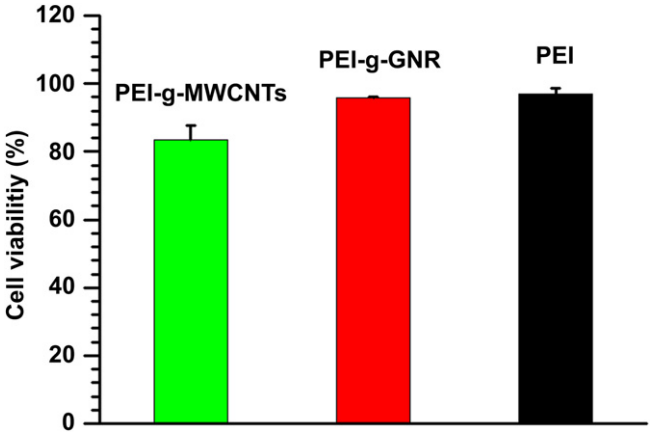

Fig. 6. Cytotoxicity induced by PEI-g-MWCNTs, PEI-g-GNR and PEI in HeLa cells.

on glass slides to detect the confocal images with a laser scanning confocal microscope (LSM-710 Zeiss, Germany).

2.8. Apoptosis experiment

The apoptosis experiments were carried out with PI staining. After the cells ($\sim 5 \times 10^4$) were seeded on glass cover slides, the culture media were replaced with media containing PEI-g-GNR conjugates for further 3 h. Afterwards, the cells were thoroughly washed and resuspended in fresh media to culture for another 24 h. The resulting cells were harvested, permeabilized with 96% ethanol and stained in 500 μL binding buffer supplemented with 5 μL PI for 10 min in dark. The HeLa cells were collected and analyzed by flow cytometry on FACSCalibur flow cytometer (Becton Dickinson, USA).

3. Results and discussion

3.1. Characterization of GNR

The TEM image of as-prepared GNR showed that after longitudinal unzipping of MWCNTs the walls of the MWCNTs were opened to a high degree (Fig. 2A). The average width of the GNR was observed to be 70–130 nm, which was just about 3.14 times of the pristine MWCNTs. The GNR showed a length distribution of about 220–400 nm, which was much shorter than the pristine MWCNTs due to the combined treatment of sonication and strong acid. The size of the GNR made it suitable to be used as a gene vector. AFM analysis of the GNR showed the typical length of 220–400 nm and width of 70–130 nm (Fig. 2B), which were in agreement with the TEM observation. As general monolayer nanostructures, the GNR showed a tendency to fold and overlap layer-by-layer (Fig. 2A and B).

Raman spectra further demonstrated the formation of GNR. As shown in Fig. 2C and D, the G band of the GNR (curve a) appeared to shift to a higher frequency and was broader than the G band of the pristine MWCNTs (curve b). Meanwhile, the D band ascribed to the presence of defects on the surface or the plane edges of GNR (curve a) increased compared to the D band of the pristine MWCNTs (curve b), which resulted in an increased D:G ratio, as reported in previous works [34,35].

3.2. Characterization of PEI-g-GNR

The FT-IR spectra and EIS analysis were employed to characterize the formation of the PEI-g-GNR. As shown in Fig. 3A, the spectrum of the PEI-g-GNR (curve a) presented the characteristic peaks of both PEI (curve b) and GNR (curve c), which indicated the successful assembly of the PEI-g-GNR. In curve a, the strong and broad absorption peak located at 3400 cm^{-1} could be attributed to the N–H bond of PEI and –OH groups in PEI and GNR, and a $-NH_2$ bending peak at 1559 cm^{-1} and a C–N stretching vibration at 1460 cm^{-1} from PEI were also observed [36]. Meanwhile, the ketone groups of GNR at 1740, 1634 cm^{-1} and peaks assigned to the

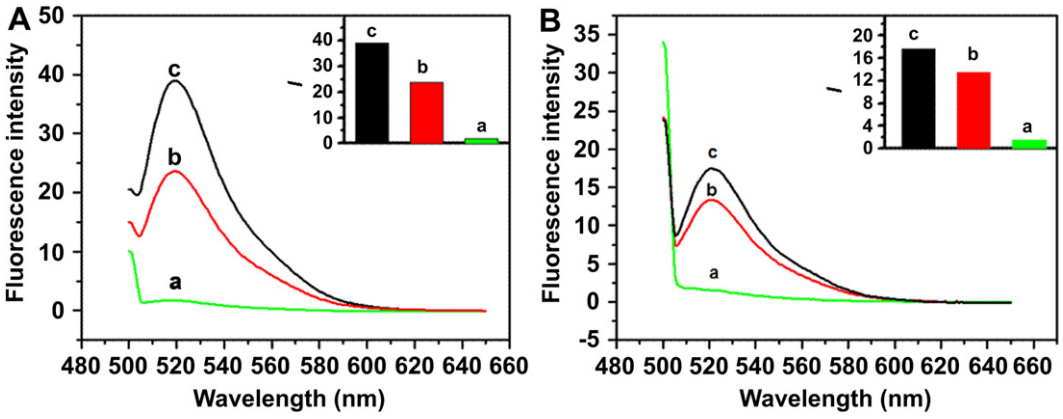

Fig. 5. Fluorescence spectra of (a) LNA-m-MB/PEI-g-GNRs, (b) LNA-m-MB and (c) MB in presence of (A) 1 U DNase I and (B) SSB at probe/SSB concentration ratio of 1:5. Insets: histograms of fluorescence intensities.

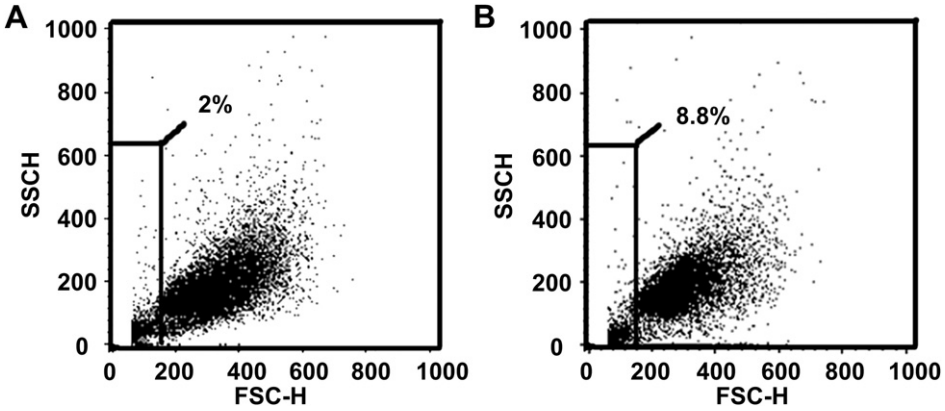

Fig. 7. Flow cytometric apoptotic analysis of (A) HeLa cells and (B) HeLa cells transfected with PEI-g-GNR.

epoxy group of the GNR at the 892, 852 cm^{-1} could be clearly observed in curve a [35].

EIS analysis is a powerful tool for monitoring the layer-by-layer assembling process [37]. Fig. 3B shows a comparison between the EIS recorded at GNR and PEI-g-GNR modified glassy carbon electrodes. The PEI-g-GNR shows an electron-transfer resistance of about 280 Ω (curve b), which is much smaller than that of GNR modified electrode (curve c). These results suggest that the PEI was successfully grafted

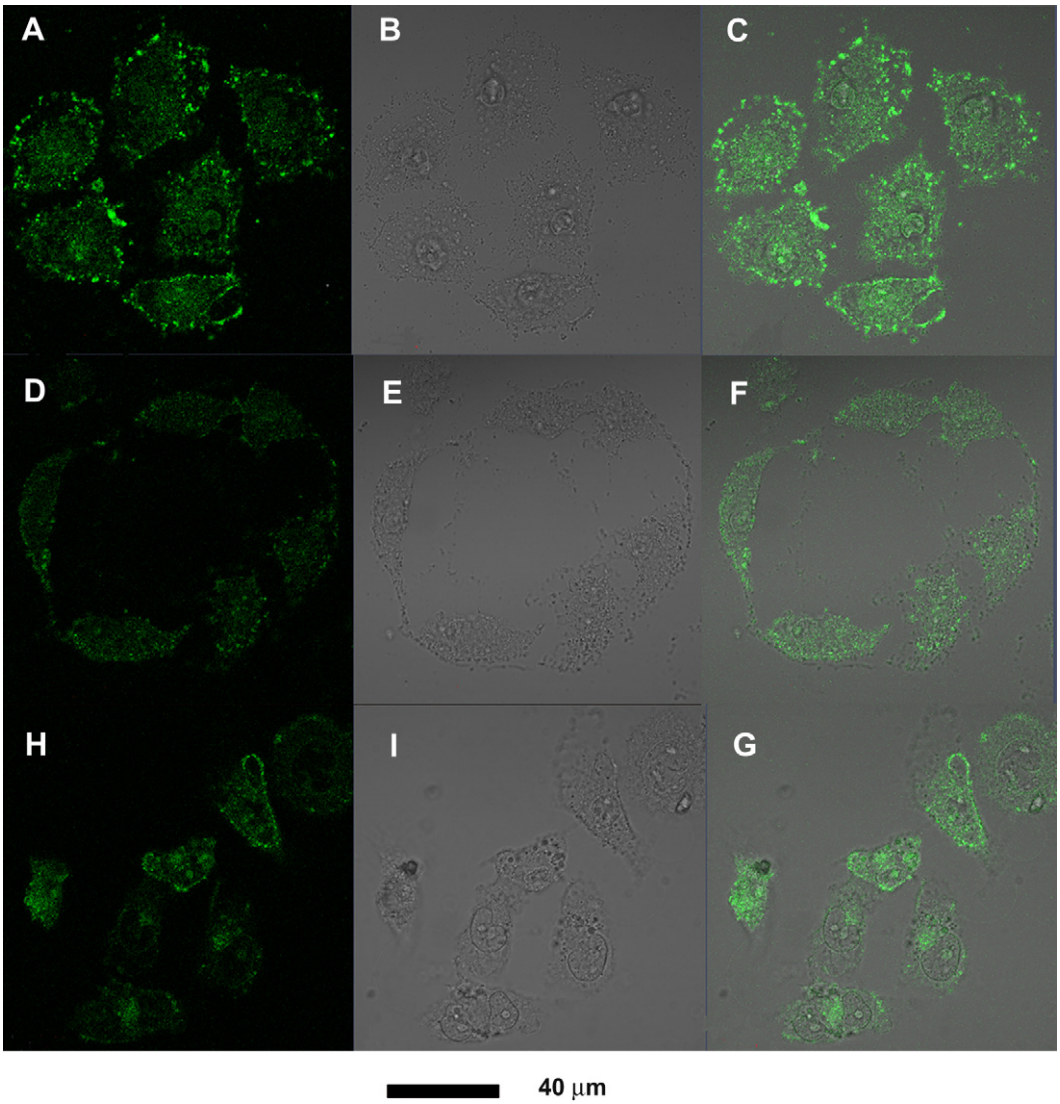

Fig. 8. Confocal images of HeLa cells after transfected with LNA-m-MB/PEI-g-GNR (A, B, C), LNA-m-MB/PEI (D, E, F) and LNA-m-MB/PEI-g-MWCNTs (G, H, I) at 37 °C for 3 h: fluorescence field (A, D, G), bright field (B, E, H) and overlapped images (C, F, I).

on GNR, the lower resistance of the PEI-g-GNR results from the positive charge of PEI on the surface of GNR, which is in favor of the electron transfer of negatively charged $Fe(CN)^{3-/4-}$ [12].

3.3. Protective properties of PEI-g-GNR

An excellent delivery vector can protect the gene cargos against nuclease digestion or SSB interaction during prolonged transport. To investigate the protective properties of the PEI-g-GNR, LNA-m-MB probes were loaded on PEI-g-GNR to form LNA-m-MB/PEI-g-GNR conjugates. As shown in Fig. 4, the conjugates presented negligible fluorescent intensity in absence of target (curve a). The low background signal of the fluorescent dye FAM resulted from a combined quenching by Dabcyl quencher and GNR. Upon addition of the target, the fluorescent dye separated from the quencher due to the hybridization, the fluorescence intensity showed a sharp enhancement (curve b), which demonstrated the well response of the LNA-m-MB/PEI-g-GNR to the target. After DNase I was added in the conjugate solution for 30 min, the fluorescence spectrum showed a low intensity of 1.77 (Fig. 5A, curve a), which was much lower than the fluorescent intensity increase of 23.9 and 39.0 observed from the fluorescence spectra of LNA-m-MB and MB as controls after addition of DNase I for the same time (Fig. 5A, curves b and c). This result indicated both LNA-m-MB and MB were degradeted, which led to the separation of the fluorescent dye molecule from the quencher. The lower fluorescent intensity increase of LNA-m-MB than MB resulted from the decreased degradation of LNA-m-MB due to the good resistance of LNA against DNase I [38]. The much weaker fluorescent intensity of the LNA-m-MB/PEI-g-GNR suggested the good protection of PEI-g-GNR from the enzymatic cleavage of LNA-m-MB.

SSB protein can nonspecifically bind to nucleic acid probe to produce false positivity [39]. So it is necessary to investigate the interaction of the LNA-m-MB/PEI-g-GNR with SSB. As shown in Fig. 5B, after SSB was added in the conjugate, LNA-m-MB and MB solutions for 30 min, the fluorescent intensity of the conjugate solution showed only 8.4% and 11.2% those of MB and LNA-m-MB solutions. This result demonstrated that PEI-g-GNR could protect LNA-m-MB from the interference of SSB, and LNA could also avoid the interference in some degree due to its unique property. Although the protective mechanism of PEI-g-GNR are not well understood, it might be explained as follows: the PEI-g-GNR could act as a shield to hinder the physical access of the nucleases/proteins to the LNA-m-MB, or the conformational change of LNA-m-MB in the presence of PEI-g-GNR made it be unrecognizable to enzyme binding pockets.

3.4. Cytotoxicity

The cytotoxicity depends on the biocompatibility of the gene vector. MTT assay was carried out to evaluate the cytotoxicity of the PEI-g-GNR. As comparison, the cytotoxicity of PEI and PEI-g-MWCNTs was also investigated with the same procedure, respectively. As shown in Fig. 6, after HeLa cells were cultivated in media containing PEI-g-GNR, PEI-g-MWCNTs, or PEI for 3 h, the PEI-g-GNR-transfected cells exhibited 95.7% viability, while the PEI-g-MWCNTs and PEI-transfected cells showed 83.4% and 96.9% viability, respectively, indicating lower cytotoxicity of PEI-g-GNR than PEI-g-MWCNTs due to the cytotoxicity of MWCNTs to HeLa cells [12]. The slight higher cytotoxicity of PEI-g-GNR than PEI was due to the aggregation of PEI on GNR, which increased the weight and size of the aggregation [40,41] and enhanced the adherence of PEI on cell surface to cause destabilization and form significant necrosis [42]. The 95.7% cell viability of PEI-g-GNR-transfected cells was higher the threshold of 90% [43], and also better than some other gene vectors [13]. Thus PEI-g-GNR could be a potential gene vector for future application in gene therapy.

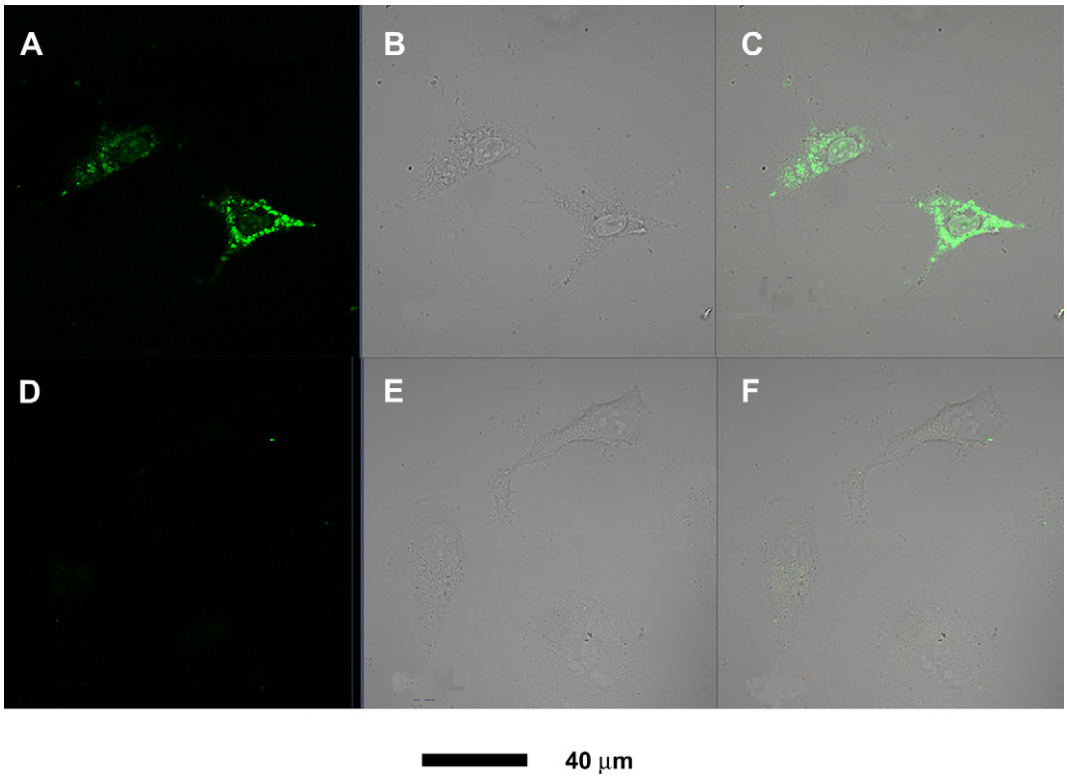

Fig. 9. Confocal images of HeLa cells after transfected with LNA-m-MB/PEI-g-GNR at 37 (A, B, C) and 4 °C (D, E, F) for 1 h: fluorescence field (A, D), bright field (B, E) and overlapped images (C, F).

The apoptosis of HeLa cells induced by PEI-g-GNR was monitored with flow cytometry analysis by PI staining (Fig. 7). Compared to control group that was incubated in absence of PEI-g-GNR and presented an apoptotic ratio of 2% (Fig. 7A), the cells transfected with PEI-g-GNR displayed slightly higher apoptotic ratio (Fig. 7B), which further suggested PEI-g-GNR could efficiently remain viability.

3.5. In vitro transfection and detection of MicroRNA

Confocal microscopic imaging was performed to assess the capability of the PEI-g-GNR as gene vector to transfer the LNA-m-MB, which possesses remarkable affinity and specificity to miRNA target, into HeLa cells for the detection of miRNA. The confocal microscopic images revealed that all of the PEI-g-GNR, PEI and PEI-g-MWCNTs could deliver the LNA-m-MB into the cells, and the target miRNA could be successfully recognized to produce green fluorescence of the dye due to the separation of the dye from the quencher labeled to MB (Fig. 8). The green fluorescent intensity depended on the amount of miRNA in cytoplasm when the same concentration of LNA-m-MB/PEI-g-GNR was used in the transfection process, producing a method for specific detection of miRNA due to the specific recognition of LNA-m-MB to miRNA.

The fluorescent intensity of the transfected cells is related to the transfection efficiency. The LNA-m-MB/PEI-g-GNR-transfected cells (Fig. 8C) exhibited much stronger intensity than those transfected with LNA-m-MB/PEI (Fig. 8F) and LNA-m-MB/PEI-g-MWCNTs (Fig. 8G). The values of fluorescent intensity of six HeLa cells transfected by above three different systems at the same condition were 165.84, 94.38 and 143.94. Thus, the mean values of a single HeLa cell transfected by above three different systems were 27.64, 15.73 and 23.99, respectively. These results suggest that the PEI-g-GNR had a higher ability to deliver the LNA-m-MB into cells. The high transfection efficiency of LNA-m-MB/PEI-g-GNR resulted from its good stability that protected the probe from degradation, and the improved proton sponge effect of PEI [13]. Compared to the MWCNTs, the GNR had larger surface area for conjugation of PEI, thus led to stronger proton-sponge effect.

Using the fluorescence labeled sequence (5′FAM-atcagtctgataagcta-3′) as model, the transfection mechanism was studied. The endocytosis mechanism sharply depended on the temperature. The HeLa cells transfected with LNA-m-MB/PEI-g-GNR at 37 °C for 1 h showed much stronger green fluorescence than those transfected at 4 °C for 1 h (Fig. 9C and F), indicating less LNA-m-MB/PEI-g-GNR conjugates entered the cells at 4 °C. This phenomenon suggested that the transfection process of LNA-m-MB/PEI-g-GNR followed an endocytosis mechanism [44,45].

4. Conclusion

A gene vector PEI-g-GNR was reported to effectively transfer the gene probe into cells. Using LNA-m-MB and HeLa cells as models, the transfer process was monitored by the confocal microscopic imaging to exhibit the specific recognition of LNA-m-MB to miRNA in cytoplasm, which led to their hybridization and strong fluorescent signal due to the separation of fluorescent dye from quencher labeled to LNA-m-MB. The PEI-g-GNR nanocarrier showed negligible cytotoxicity and could protect the LNA-m-MB from nuclease digestion or SSB interaction. The enhanced proton-sponge effect of PEI led to relatively high transfection efficiency, which was favorable to the sensitive detection of the recognized target miRNA. The proposed PEI-g-GNR would be a promising nonviral vector in future gene therapy and clinical application.

Acknowledgment

This work was financially supported by National Natural Science Foundation of China (90713015, 20875044, 20821063, 21075055), National Basic Research Program (2010CB732400), the Outstanding Medical Talents Program (RC2007069) from Department of Health of Jiangsu, and Natural Science Foundation of Jiangsu (BK2008014).

References

[1] Zelphati O, Szoka FC. Mechanism of oligonucleotide release from cationic liposomes. Proc Natl Acad Sci U S A 1996;93:11493–8.
[2] Boussif O, Lezoualc'h F, Zanta MA, Mergny MD, Scherman D, Demeneix B, et al. A versatile vector for gene and oligonucleotide transfer into cells in culture and in vivo: polyethylenimine. Proc Natl Acad Sci U S A 1995;92:7297–301.
[3] Okuda T, Sugiyama A, Niidome T, Aoyagi H. Characters of dendritic poly(l-lysine) analogues with the terminal lysines replaced with arginines and histidines as gene carriers in vitro. Biomaterials 2004;25:537–44.
[4] Lo SL, Wang S. An endosomolytic tat peptide produced by incorporation of histidine and cysteine residues as a nonviral vector for DNA transfection. Biomaterials 2008;29:2408–14.
[5] Singh R, Pantarotto D, McCarthy D, Chaloin O, Hoebeke J, Partidos CD, et al. Binding and condensation of plasmid DNA onto functionalized carbon nanotubes:toward the construction of nanotube-based gene delivery vectors. J Am Chem Soc 2005;127:4388–96.
[6] Behr JP. Synthetic gene-transfer vectors. Acc Chem Res 1993;26:274–8.
[7] Liu Z, Winters M, Holodniy M, Dai HJ. siRNA delivery into human T cells and primary cells with carbon-nanotube transporters. Angew Chem Int Ed 2007;46:2023–7.
[8] Rosi NL, Giljohann DA, Thaxton CS, Lytton-Jean AKR, Han MS, Mirkin CA. Oligonucleotide-modified gold nanoparticles for intracellular gene regulation. Science 2006;312:1027–30.
[9] Jia NQ, Lian Q, Shen HB, Wang C, Li XY, Yang ZN. Intracellular delivery of quantum dots tagged antisense oligodeoxynucleotides by functionalized multiwalled carbon nanotubes. Nano Lett 2007;7:2976–80.
[10] Liu Y, Wu DC, Zhang WD, Jiang X, He CB, Chung TS, et al. Polyethylenimine-grafted multiwalled carbon nanotubes for secure non-covalent immobilization and efficient delivery of DNA. Angew Chem Int Ed 2005;44:4782–5.
[11] Kosynkin1 DV, Higginbotham1 AL, Sinitskii1 A, Lomeda1 R, Dimiev A. Longitudinal unzipping of carbon nanotubes to form graphene nanoribbons. Nature 2009;458:872–6.
[12] Li XL, Wang XR, Zhang L, Lee SW, Dai HJ. Chemically derived, ultrasmooth graphene nanoribbon semiconductors. Science 2008;319:1229–32.
[13] Barone V, Hod O, Scuseria GE. Electronic structure and stability of semiconducting graphene nanoribbons. Nano Lett 2006;6:2748–54.
[14] Neu M, Fischer D, Kissel T. Recent advances in rational gene transfer vector design based on poly(ethyleneimine) and its derivatives. J Gene Med 2005;7:992–1009.
[15] Akinc A, Thomas M, Klibanov AM, Langer R. Exploring polyethylenimine mediated DNA transfection and the proton sponge hypothesis. J Gene Med 2005;75:657–63.
[16] Schäfer J, Höbel S, Bakowsky U, Aigner A. Liposome-polyethylenimine complexes for enhanced DNA and siRNA delivery. Biomaterials 2010;31:4771–80.
[17] Wang CF, Lin YX, Jiang T, He F, Zhuo RX. Polyethylenimine-grafted polycarbonates as biodegradable polycations for gene delivery. Biomaterials 2009;30:4824–32.
[18] Koshkin AA, Nielsen P, Meldgaard M, Rajwanshi VK, Singh SK, Wengel J. LNA (locked nucleic acid): an RNA mimic forming exceedingly stable LNA: LNA duplexes. J Am Chem Soc 1998;120:13252–3.
[19] Koshkin AA, Rajwanshi VK, Wengel J. Novel convenient syntheses of LNA [2.2.1] bicyclo nucleosides. Tetrahedron Lett 1998;39:4381–4.
[20] Lu J, Tsourkas A. Imaging individual microRNAs in single mammalian cells in situ. Nucleic Acids Res 2009;37(14):e100.
[21] Kloosterman WP, Wienholds E, de Bruijn E, Kauppinen S, Plasterk RH. In situ detection of miRNAs in animal embryos using LNA-modified oligonucleotide probes. Nat Methods 2006;3:27–9.
[22] Nuovo GJ, Elton TS, Nana-Sinkam P, Volinia S, Croce CM, Schmittgen TD. A methodology for the combined in situ analyses of the precursor and mature forms of microRNAs and correlation with their putative targets. Nat Protoc 2009;4:107–15.
[23] Landgraf P, Rusu M, Sheridan R, Sewer A, Iovino N, Aravin A. A mammalian microRNA expression atlas based on small RNA library sequencing. Cell 2007;129:1401–14.
[24] Cao X, Yeo G, Muotri AR, Kuwabara T, Gage FH. Noncoding RNAs in the mammalian mentral nervous system. Annu Rev Neurosci 2006;229:77–103.
[25] Bartel DP. MicroRNAs: genomics, biogenesis, mechanism, and function. Cell 2004;116:281–97.
[26] Brennecke J, Hipfner DR, Stark A, Russell RB, Cohen SM. bantam encodes a developmentally regulated microRNA that controls cell proliferation and regulates the proapoptotic gene hid in drosophila. Cell 2003;113:25–36.

[27] Kloosterman WP, Plasterk RH. The diverse functions of microRNAs in animal development and disease. Dev Cell 2006;11:441–50.
[28] Garzon R, Fabbri M, Cimmino A, Calin GA, Croce CM. MicroRNA expression and function in cancer. Trends Mol Med 2006;12:580–7.
[29] Wark AW, Lee HJ, Corn RM. Multiplexed detection methods for profiling microRNA expression in biological samples. Angew Chem Int Ed 2008;47:644–52.
[30] Cissell KA, Shrestha S, Deo SK. Bioluminescence-based detection of MicroRNA, miR21 in breast cancer cells. Anal Chem 2007;79:4754–61.
[31] Nelson T, Zhang B, Prezhdo OV. Detection of nucleic acids with graphene nanopores: ab initio characterization of a novel sequencing device. Nano Lett 2010;10:3237–42.
[32] Mawhinney DB, Naumenko V, Kuznetsova A, Yates JT, Liu J, Smalley RE. Surface defect site density on single walled carbon nanotubes by titration. Chem Phys Lett 2000;324:213–6.
[33] Hu H, Bhowmik P, Zhao B, Hamon MA, Itkis ME, Haddon RC. Determination of the acidic sites of purified single-walled carbon nanotubes by acid-base titration. Chem Phys Lett 2001;345:25–8.
[34] Higginbotham AL, Kosynkin DV, Sinitskii A, Sun ZZ, Tour JM. Lower-defect graphene oxide nanoribbons from multiwalled carbon nanotubes. ACS Nano 2010;4:2059–69.
[35] Cataldo F, Compagnini G, Patané G, Ursini O, Angelini G, Ribic PR, et al. Graphene nanoribbons produced by the oxidative unzipping of single-wall carbon nanotubes. Carbon 2010;48:2596–602.
[36] Hu Y, Cai KY, Luo Z, Hu R. Construction of polyethyleneimine-β-cyclodextrin/pDNAmultilayer structure for improved in situ gene transfection. Adv Eng Mater 2010;12:B18–25.
[37] Deng SY, Jian GQ, Lei JP, Hu Z, Ju HX. A glucose biosensor based on direct electrochemistry of glucose oxidase immobilized on nitrogen-doped carbon nanotubes. Biosens Bioelectron 2009;25:373–7.
[38] Schmidt KS, Borkowski1 S, Kurreck J, Stephens AW, Bald R, Hecht M, et al. Application of locked nucleic acids to improve aptamer in vivo stability and targeting function. Nucleic Acids Res 2004;32:5757–65.
[39] Wu YR, Phillips JA, Liu HP, Yang RH, Tan WH. Carbon nanotubes protect DNA strands during cellular delivery. ACS Nano 2008;2:2023–8.
[40] Godbey WT, Wu KK, Mikos AG. Poly(ethylenimine) and its role in gene delivery. J Control Release 1999;60:149–60.
[41] Fischer D, Li Y, Ahlemeyer B, Krieglstein J, Kissel T. In vitro cytotoxicity testing of polycations: influence of polymer structure on cell viability and hemolysis. Biomaterials 2003;24:1121–31.
[42] Fischer D, Bieber T, Li Y, Elsasser HP, Kissel T. A novel non-viral vector for DNA delivery based on low molecular weight, branched polyethylenimine: effect of molecular weight on transfection efficiency and cytotoxicity. Pharm Res 1999;16:1273–9.
[43] Choksakulnimitr S, Masuda S, Tokuda H, Takakura Y, Hashida M. In vitro cytotoxicity of macromolecules in different cell culture systems. J Control Release 1995;34:233–41.
[44] Cherukuri P, Bachilo SM, Litovsky SH, Weisman RB. Near-infrared fluorescence microscopy of single-walled carbon nanotubes in phagocytic cells. J Am Chem Soc 2004;126:15638–9.
[45] Kam NWS, Jessop TC, Wender PA, Dai HJ. Nanotube molecular transporters: internalization of carbon nanotube-protein conjugates into mammalian cells. J Am Chem Soc 2004;126:6850–1.